

Numerical Study of Aerodynamic Performance of Airfoil with Variable Curvature Split Flap

S. Huang¹, H. Qiu² and Y. Wang^{1,3†}

¹ School of Energy and Power Engineering, University of Shanghai for Science and Technology 2, Shanghai, 200093, China

² Department of Mechanical and Aerospace Engineering, The Hong Kong University of Science and Technology, Hong Kong

³ National Key Laboratory of Science and Technology on Aerodynamic Design and Research, Xi'an, 710072, China

†Corresponding Author Email: wangying@usst.edu.cn

(Received September 4, 2022; accepted February 1, 2023)

Abstract

To further improve the lift-rising effect of the attached flap on an airfoil, based on the unique movement pattern of a fluke when a dolphin moves forward, this paper puts forward a novel attached split flap model with variable curvature. The lift-type vertical axis wind turbine's typical blade airfoil NACA 0018 is taken as the research object. First, the aerodynamic performance of the two-dimensional airfoil is simulated based on the SST $k-\omega$ turbulence model. The contrast between the simulation and the experimental results proves the correctness of the numerical simulation methods in this paper. Then, the effectiveness of split flap is verified, and the lift-rising principle is briefly analyzed. Finally, the parametric study is carried out based on the flap model with variable curvature proposed in this paper, and the lift-rising principle of the variable curvature split flap is analyzed in detail. The results indicate that, with the rise of the flap's curvature index, the airfoil's lift coefficient (C_l) integrated with the flap gradually increases accordingly and tends to a constant value. The bionic research in this paper can provide a comprehensive reference for the aerodynamic shape design of airfoil trailing edge flap and the further optimization of energy efficiency of rotating machinery or aviation.

Keywords: Split flap; Variable curvature; Vertical axis wind turbine; Flow control; Parameter optimization.

1. INTRODUCTION

Whether in the field of rotating machinery or aviation, airfoil lift-rising technology has always been an important research direction in fluid mechanics. Especially for the lift-type vertical axis wind turbine, the lift obtained by the blade directly determines the energy efficiency of the turbine.

To improve the lift of airfoils and optimize the performance of VAWTs, researchers have adopted various flow control methods. Kral (2000) proposed to divide the flow control technology into two categories, including passive and active control. Appropriate flow control approaches on an airfoil can significantly improve its aerodynamic performance. Generally speaking, the passive control method is relatively simple in form and structure and has no external energy injection. It mainly includes the methods of setting a flat plate or a small cylinder at the front end of the blade (Zhou *et al.* 2017; Wang *et al.* 2018), setting a vortex generator (Wang *et al.* 2017), setting slotting

or drilling holes in some parts of the airfoil (Liu and Tan 2018), etc. Unlike the passive control methods, the active control methods are more flexible because they can be adjusted according to the actual situation. The corresponding techniques mainly include blowing and sucking in the boundary layer (Zhang *et al.* 2017; Fatahian *et al.* 2019), synthetic jet (Feero *et al.* 2017; Velasco *et al.* 2017), adding plasma generator near the leading edge of airfoil (Post and Corke 2006; Bénard *et al.* 2009) and so on.

Actually, in the majority of research on airfoil lift-rising, flaps have been widely used (Urnes and Nguyen 2013; Kaul and Nguyen 2014) due to their apparent advantages of simple structure and high lift-rising efficiency. The flap lift-rising devices can be roughly divided into leading edge and trailing edge lift-rising devices in terms of layout. The leading edge lift-rising devices of the flap are mainly used in the situation of being at a high attack angle, such as leading edge flap slot (Weick and Platt 1933), leading edge flap (Melton *et al.* 2005),

Kruger flap (Kulhánek *et al.* 2020) and slot leading edge flap (Atalay *et al.* 2020), as shown in Fig. 1. These methods change the relative angle between incoming flow and airfoil, which aims at delaying stall and improving the lift of airfoil at high attack angle. The trailing edge lift-rising devices of the flap are widely used further, such as simple flaps (Kim *et al.* 2020), split flaps (Duong *et al.* 2020), single-slotted or multi-slotted flaps (Duong *et al.* 2020) and Gurney flaps (Li *et al.* 2020), as shown in Fig. 2, where the trailing edge flap has more significant lift-rising effect both before and after stall conditions.

Ultimately, in the above technology of increasing airfoil lift with flaps, many methods have been used to optimize the energy efficiency of Vertical Axis Wind Turbines (VAWTs). Zhang *et al.* (2021) installed the split flap on the airfoil, and it was found that the efficiency of the VAWT was increased by 5.8%. Zhu *et al.* (2019) proposed a new application mode of the Gurney flap, which increased the energy efficiency of VAWT by 19.72%. Since Darrieus turbines are not self-starting, the slotted flap was applied to the Darrieus wind turbine by Daróczy *et al.* (2014), and a good improvement effect was obtained.

Figure 3 shows the appearance comparison of dolphin fluke in states of station and propulsion. As shown in Fig. 3(a), in the static condition, the fluke extends horizontally along the dolphin body direction, which is almost in a straight line. In the propulsion state, as shown in Fig. 3(b), due to the unique flexible characteristic of dolphin fluke, the fluke would be deformed in the process of beating

water up and down, and its appearance is similar to a bowl-shaped surface (Schaefer 2008).

Compared with the flat and straight dolphin fluke at static state in Fig. 3(a), the bowl-shaped fluke can catch and drain more water, which makes the dolphin fluke get more thrust (Schaefer 2008). Fish *et al.* (2018) took similar pictures in the experiment studying the power source of dolphins, as shown in Fig. 4 below.

Given the relationship between propulsion and energy acquisition, this paper speculated that the curvature of the flap could be changed by imitating the bowl-shaped water-catching shape of the dolphin fluke based on previous research on original flaps, to further optimize the aerodynamic efficiency of the original airfoil integrated with flap. Therefore, inspired by the bowl-shaped dolphin fluke during propulsion, this paper puts forward a mathematical model changing flap's curvature, and applies this model to the split flap due to its simple structure, as shown in Fig. 3 and Fig. 4. By changing the curvature of the split flap, the corresponding influence on the aerodynamic efficiency of the airfoil and the curved flap itself is then studied.

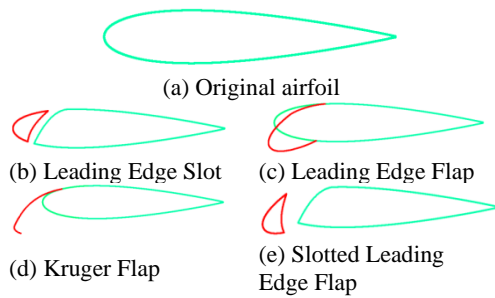


Fig. 1 Leading edge lift-rising devices of flap.

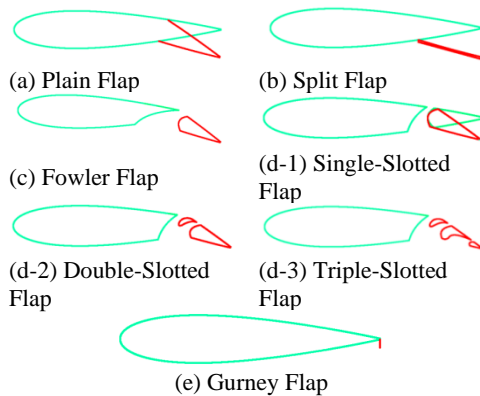
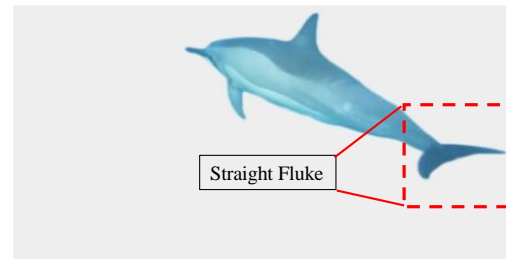
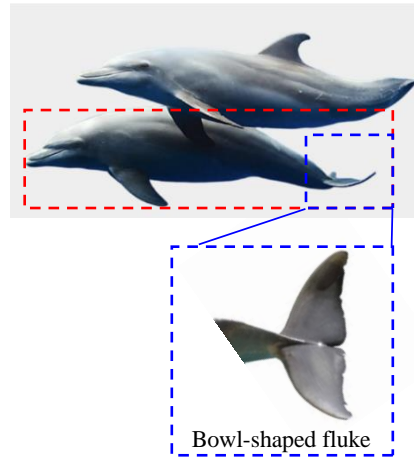


Fig. 2. Trailing edge lift-rising devices of flap.



(a) Static fluke



(b) Shape variation of fluke during propulsion
Fig. 3. Schematic diagram of dolphin fluke.

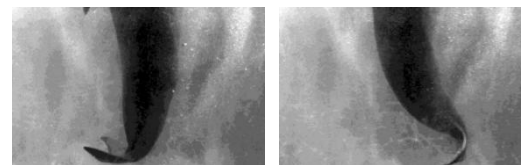


Fig. 4. Dolphin fluke during propulsion (Schaefer 2008).

The novelty of the present study can be summarized as follows:

(1) The effect of various flaps on the optimization of airfoil aerodynamic performance and the improvement of wind turbine efficiency has been fully proved. However, the new method to further improve the overall aerodynamic performance optimization effect of existing flaps or airfoils has not been fully developed. Taking a split flap as an example, this paper proposes a curved split flap based on a bowl-shaped dolphin fluke during propulsion, which can further effectively optimize the aerodynamic efficiency of the original flap.

(2) Among some new methods to further improve the performance optimization effect of existing flaps, the flap deflection angle has actually changed. In this paper, the premise that the flap deflection angle remains unchanged is strictly guaranteed, and the purpose of optimizing the overall aerodynamic performance of the airfoil and the flap is achieved only by rearranging the local deflection angle of the traditional flap.

(3) There are diverse methods in the installation and deformation of trailing edge flaps. However, in most studies on flaps, the efficiency of flap's curvature on the overall aerodynamic performance of airfoils is rarely considered. Better aerodynamic performance may be achieved by changing the curvature of the contact surface between the flap and fluid.

(4) The novel mathematical model of the curved flap is creatively developed. The optimal deformation parameters of the curved flap are determined through parametric research.

2. CALCULATION MODEL

In this paper's situation, the NACA0018 airfoil is used as the basic airfoil, and the chord length (C) of the airfoil is set as 1m, and a rigid hinged plate with a length of $L= 3\%C$ is horizontally arranged on the lower surface at $97\%C$. The red dotted line in Fig. 5(a) shows the original position of the split flap. $S(x_0, y_0)$ is the hinged point between the flap and the original NACA0018 airfoil surfaces. In addition, the definition of the flap height (H) is shown in Fig. 5(b). Liebeck (1978) believed when the flap height exceeds 2% of the airfoil chord length, the resistance increases obviously. Bianchini *et al.* (2019) found that, through numerical simulation, the flap height should not be too large, otherwise it adversely affects the overall lift-to drag coefficient of the airfoil and the flap. Li *et al.* (2020) found that, through experiments, when the flap height is $2\%C$, the effectiveness of the flap is relatively higher. Based on the conclusion of previous literature and the Reynolds numbers selected in this paper ($Re=1.6 \times 10^5$), $2\%C$ is chosen as the flap height H .

2.1 Original Split Flap Model

The final position of the split flap in Fig. 5(b) can be obtained by controlling the surface nodes of the

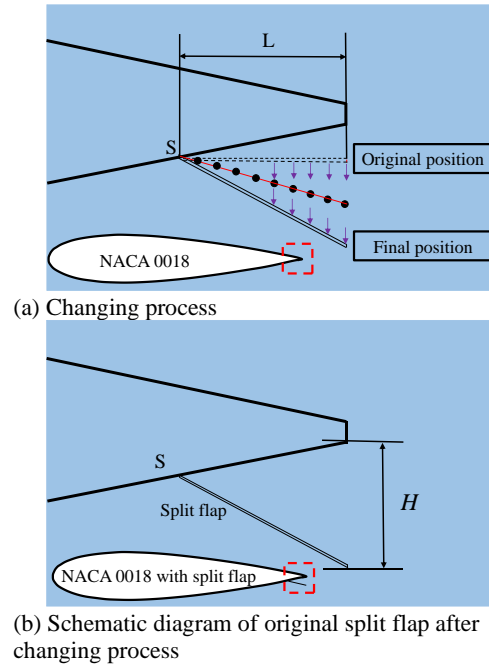


Fig. 5. Original split flap.

horizontal split flap to move downwards. In Fig. 5(b), it defines the acquisition process of the original split flap, as shown in equations (1)~(3). The original horizontal flap has a node coordinate of (x_i, y_j) , the changed flap has a node coordinate of $(NODE_X, NODE_Y)$, and it further defines the curvature coefficient k . V is the structure pointer toward the flap surface coordinates.

The flap model obtained by equations (1)~(3) in Fig. 5(b) is the original split flap model adopted in this paper, which is recorded as the Original Split Flap (OSF).

$$k = (1 / 0.03)(x_i - 0.97) \quad (1)$$

$$NODE_X(v) = x_i \quad (2)$$

$$NODE_Y(v) = y_j - Hk \quad (3)$$

2.2 Curved Split Flap Model

The acquisition process of the curved split flap is as shown in equations (4)~(5), which is similar to the acquisition process of the original split flap in section 2.1. The curved split flap is also obtained by moving the nodes on the original horizontal flap to move downwards.

Through changing values of n in equation (4), the curvature coefficient (k) can be controlled accordingly. When n is 2, the curved flap is shown in Fig. 6, which is recorded as Curved Flap- $n2$, abbreviated as CF $n2$. When n is 4, the curved flap is recorded as CF $n4$, and so on. In this paper, n is taken as 2, 4, 8, and 16, respectively. Flap with four

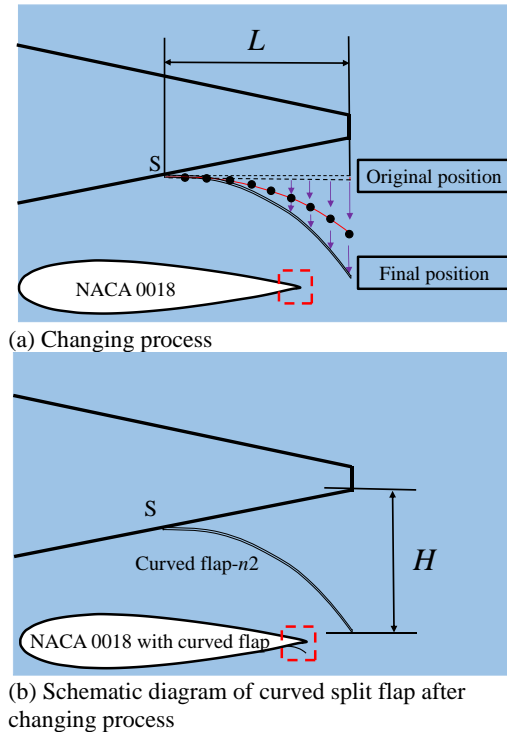


Fig. 6. Curved split flap.

curvatures is recorded as CFn2, CFn4, CFn8, and CFn16, respectively.

In this paper, the deformation height of the original split flap and the curved flap are both H . The included angle between connecting line (i.e. connecting line between leading edge point and trailing edge point of flap) and horizontal direction (i.e. direction of incoming flow) is positioned as the flap deflection angle. Notably, the deflection angles of the two flaps are consistent.

$$k = (1 / 0.03)^n (x_i - 0.97)^n \quad (4)$$

$$NODE_X(v) = x_i \quad (5)$$

$$NODE_Y(v) = y_j + Hk \quad (6)$$

2.3 Calculation Method

In Fig. 7, the grid for the original airfoil NACA0018 and the detailed grid distribution are shown. The quadrilateral grid and O-shape topology are embraced for the numerical reenactment lattice of the single two-dimensional airfoil. This paper takes the vertical axis wind turbine as the research object and the Reynolds number is $Re=1.6 \times 10^5$. The external boundary of the computational space is around 50 times of chord lengths away from the airfoil surface. To ensure $y^+ < 1$, the grid height of the first layer near the airfoil is set as $1.2 \times 10^{-4}m$, and the development proportion of the ordinary framework close to the wall is controlled within 1.1.

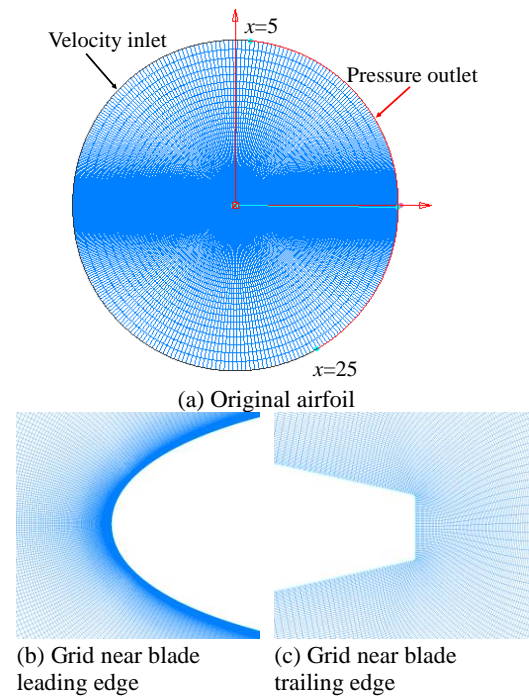


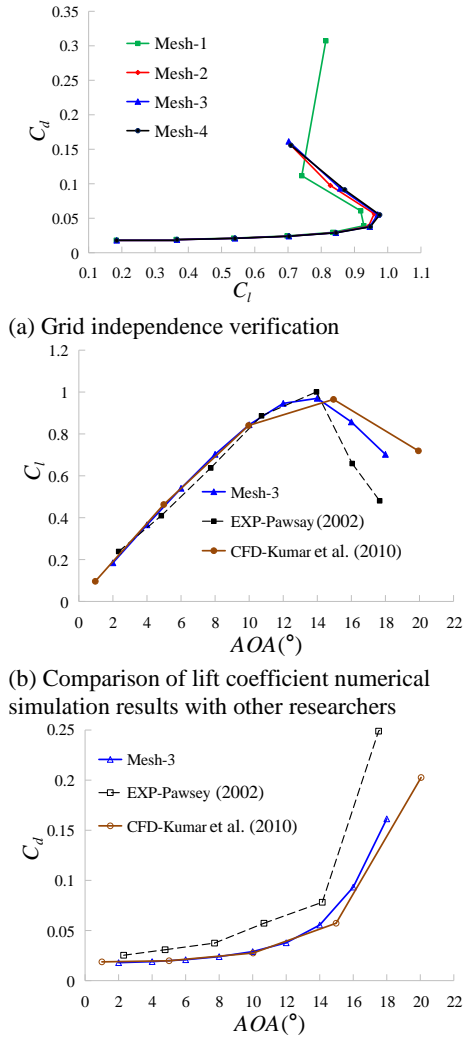
Fig. 7. Grid for original airfoil NACA0018

The velocity inlet and pressure outlet are adopted as boundary conditions and the divided area is shown in Fig. 7.

3. VERIFICATION OF CALCULATION METHOD

The grid independence verification method of the original airfoil can be referred to the previously published literature (Huang *et al.* 2021). Four sets of grids with different numbers of grids are selected for comparative analysis, and the number of grids is 63000, 127000, 191000 and 255000, represented by Mesh-1, Mesh-2, Mesh-3 and Mesh-4, respectively. According to previous experience (Huang *et al.* 2021), to save the calculation cost, in the numerical simulation study of this paper, the steady state is used for calculation before the stall occurs on the airfoil surface, and the transient state is used for calculation after the stall. When $Re=1.6 \times 10^5$, the above four kinds of grids are used to simulate the lift and drag coefficients with attack angles of 0° to 18° , and the result is shown in Fig. 8(a). Overall, the trend of calculation results of Mesh-2, Mesh-3 and Mesh-4 is close. Meanwhile, the calculation error between Mesh-3 and Mesh-4 is less than 1%. To sum up, the third grid is identified as the benchmark grid for subsequent calculation.

In addition, the numerical simulation results of the above third grid are compared with experimental results (Pawsey 2002) and simulation results (Kumar *et al.* 2010). The schematic diagram of the results are shown in Fig. 8(b) and Fig. 8(c), where the variation trend of the lift and drag coefficient is basically consistent with the experimental results. In addition,



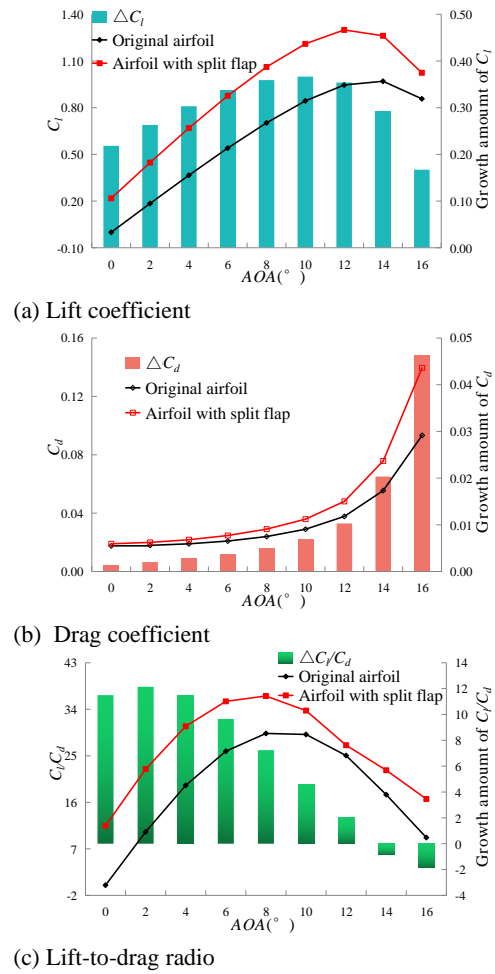
(a) Grid independence verification
(b) Comparison of lift coefficient numerical simulation results with other researchers
(c) Comparison of drag coefficient numerical simulation results with other researchers
Fig. 8. Verification of calculation method.

the error of simulation results in this paper is smaller than that of [Kumar *et al.* \(2010\)](#).

Generally speaking, the numerical simulation method is feasible and the results are effective and within the allowable error range.

4. RESULTS AND ANALYSIS

In this section, the original split flap and split flap with four kinds of curvature are numerically calculated at the attack angle range of 2°-14°. Firstly, the aerodynamic performance of NACA0018 integrated with the original split flap are compared with the original NACA0018 airfoil, and the lift-rising effect of the split flap is investigated. Besides, the lift-rising principle of the split flap is briefly analyzed. Then, the aerodynamic performance of NACA0018 with a curved split flap with four kinds of curvature are compared with that of the NACA0018 with the original split flap. Thus, the influence of different flap's curvatures on the airfoil and the flap itself are analyzed.

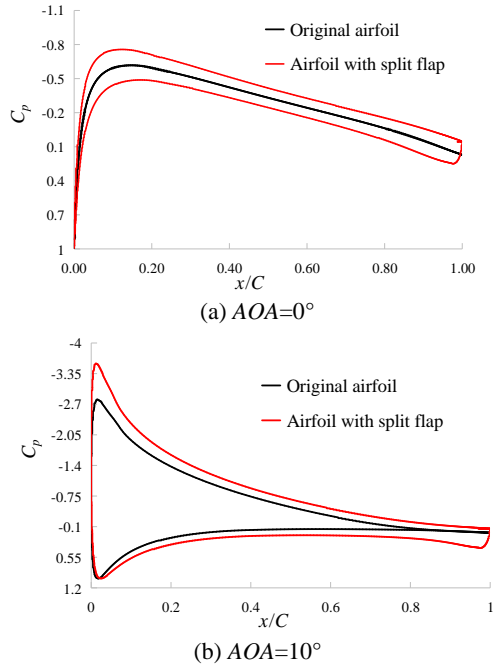
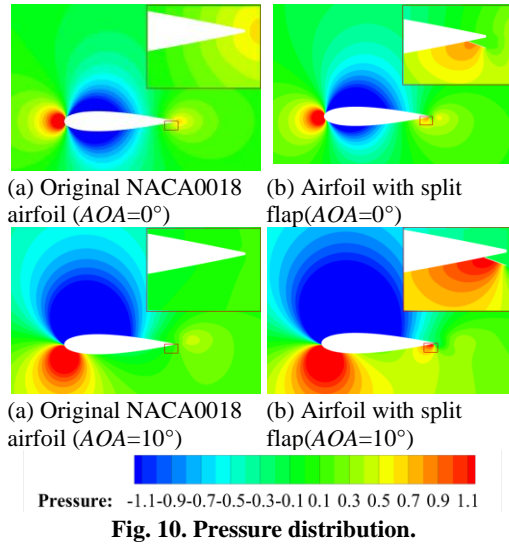


(a) Lift coefficient
(b) Drag coefficient
(c) Lift-to-drag ratio
Fig.9. Aerodynamic performance of NACA0018 with original split flap.

4.1 NACA0018 with Original Split Flap

Figure 9 shows the aerodynamic performance of the NACA0018 airfoil and NACA0018 integrated with the original split flap when the attack angle is 0°-14°. The lift coefficients of NACA0018 integrated with split flap are larger than that of NACA0018, and the drag coefficients do not increase obviously before the stall angle of attack. In addition, compared with the original NACA0018 airfoil's lift-to-drag ratio, the NACA0018 airfoil integrated with split flap is significantly improved before the stall.

The split flap changes the original flow direction of the airflow on the lower surface and deflects the airflow downward. The airflow suddenly changing the original motion direction produces an upward reaction force on the split flap. As shown in Fig. 10, compared with the original NACA0018 airfoil, the upward reaction force generated by airflow on the split flap causes the pressure near the lower surface of the split flap to increase locally. In addition, as shown in Fig. 10, the lower pressure area on the upper surface and the high pressure area on the lower surface of NACA0018 airfoil with split flap both enlarge. It indicates that the flap would influence the pressure distribution of the airfoil and is manifested by the outward motion of the pressure coefficient



curve in Fig. 11. That is, there shows the increase of airfoil circulation.

Figure 12 shows the velocity distribution of boundary layer on suction surface of the airfoil based on the 90% chord length of airfoil, and the data results are normalized. It can be seen from the figure that, compared with the air velocity on the suction surface of the NACA0018, the air velocity on the suction surface of the airfoil integrated with the original split flap rises significantly, resulting in a growth in the overall circulation and lift coefficient of the airfoil. In Fig. 12(a), at the 90%*C* of the NACA0018, the boundary layer thickness is about 3%*C* of the airfoil, so the split flap height $H=2\%C$ would not cause an increase in drag coefficient because the whole flap is in the boundary layer, which is consistent with the calculated curves in Fig. 9.

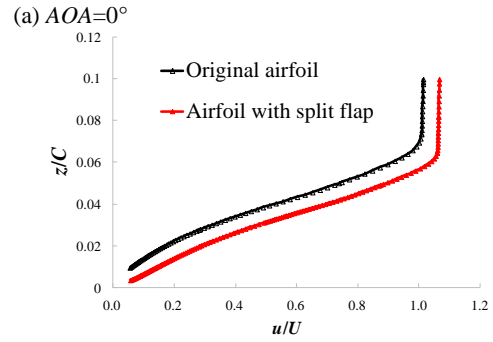
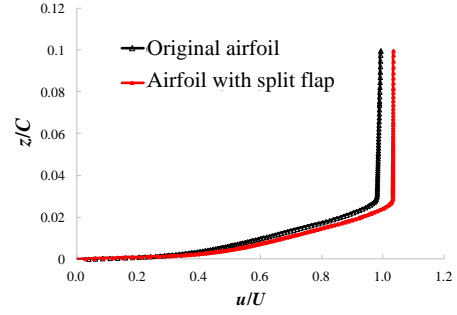


Fig. 12. Boundary layer velocity.

4.2 NACA0018 with Curved Split Flap

This section imitates the method of increasing the drainage volume of bowl-shaped dolphin fluke during propulsion. Based on the original split flap, the curvature of the flap is changed according to the curved flap model proposed in section 2.2, to further optimize the aerodynamic performance of the airfoil integrated with flap.

The lift coefficient of the airfoil integrated with the original split flap is recorded as $Cl_{OSF+airfoil}$, and the lift coefficient of the airfoil integrated with curved split flap is recorded as $Cl_{CFn+airfoil}$. If the curvature index $n=2$, the lift coefficient is recorded as $Cl_{CFn2+airfoil}$. The ordinate of Fig. 13(a) shows the lift coefficient growth rate of the airfoil integrated with flap with different camber indexes based on $Cl_{OSF+airfoil}$, and the calculation equation is:

$$\frac{Cl_{CFn+airfoil} - Cl_{OSF+airfoil}}{Cl_{OSF+airfoil}} \quad (7)$$

Similarly, the ordinate equation in Fig. 13(b) is:

$$\frac{Cl_{CFn+airfoil} / Cd_{CFn+airfoil} - Cl_{OSF+airfoil} / Cd_{OSF+airfoil}}{Cl_{OSF+airfoil} / Cd_{OSF+airfoil}} \quad (8)$$

In Fig. 13(a), the lift coefficients of the airfoil integrated with flap varying with different curvatures are higher than those of airfoils integrated with original split flap. That is, compared with original split flap, the lift coefficients of the airfoil integrated with a curved split flap imitating dolphin flukes are improved to some extent. At the same attack angle,

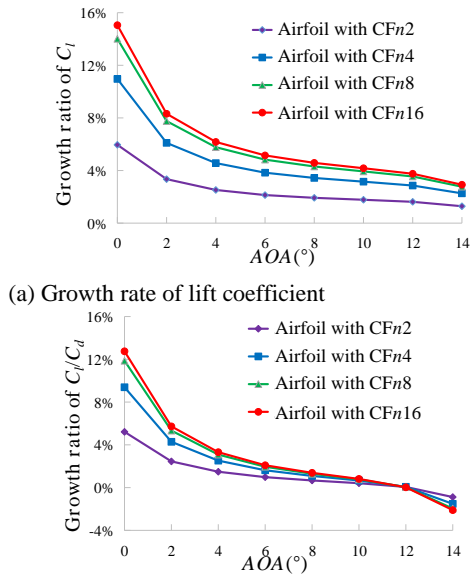


Fig. 13. The growth rates with different curvature indexes.

with the rise of the curvature index n , the lift coefficient increases by 15.05% at most. The lift-to-drag ratio in Fig. 13(b) can be increased by 12.75%. The growth rate of lift-to-drag ratio of airfoil integrated with curved flap shows a similar trend to the growth rate of lift coefficient in Fig. 13(a). Thus, the following contents of this section only consider lift coefficient as the standard for the effectiveness of flap's curvature.

It is not difficult to find from Fig. 13(a) that the lift coefficient growth rate is negatively correlated with the attack angle. With the increase of the attack angle, the lift coefficient growth rate gradually decreases. However, at a small attack angle, the lift coefficient of the airfoil integrated with flap is low. Therefore, only by the growth rate of lift coefficient, it is difficult to fully grasp the increasing effect of flap's curvature on the aerodynamic performance of the airfoil. Therefore, both the growth rate of lift coefficient and the growth amount of lift coefficient are taken as the basis for judging the flap lift-rising performance in Fig. 14. The main coordinate axis in Fig. 14 represents the lift coefficient growth rate of the airfoil integrated with a curved flap. The corresponding equation is:

$$\frac{C_{l_{CFn+airfoil}} - C_{l_{OSF+airfoil}}}{C_{l_{OSF+airfoil}}} \quad (9)$$

The secondary coordinate axis represents the growth amount of lift coefficient of airfoil integrated with a curved flap, and the calculation equation is:

$$C_{l_{CFn+airfoil}} - C_{l_{OSF+airfoil}} \quad (10)$$

In Fig. 14, when the curvature index n is determined, the lift coefficient growth rate and lift coefficient growth amount of the airfoil integrated with flap show different variation rules. The lift coefficient

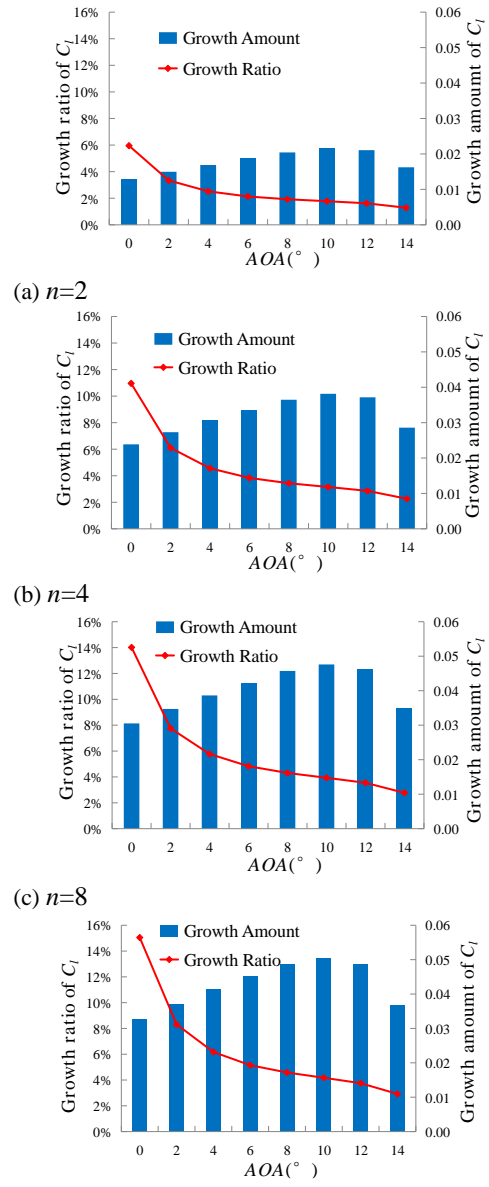
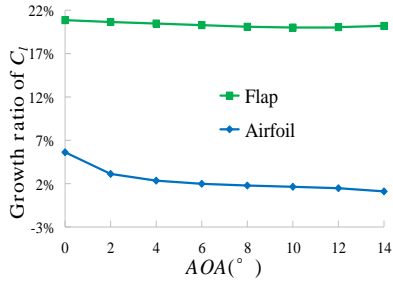


Fig.14. Growth rate and growth amount of lift coefficient under different curvature indexes.

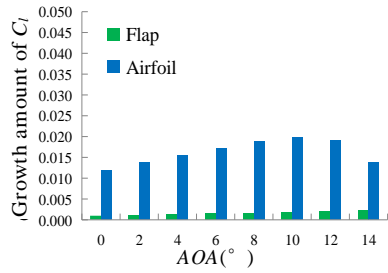
growth rate is negatively correlated with the attack angle. With the rise of the attack angle, the lift coefficient growth rate decreases continuously. With the increase of attack angle, the growth amount of lift coefficient first increases and then decreases. Besides, when the attack angle is near the stall attack angle, the growth amount of lift coefficient ($C_{l_{CFn+airfoil}} - C_{l_{OSF+airfoil}}$) reaches the maximum value.

4.3 Lift Rising Mechanism of Flap

In section 4.1, it is found that the original split flap would not only cause local high pressure of the flap, but also affect the pressure distribution and circulation change on the airfoil surface. In section 4.2, it is also found that the lift coefficient transforms after changing the flap's curvature. To explore the change of curvature on the lift coefficient of the



(a) Growth rate of lift coefficient



(b) Growth amount of lift coefficient

Fig. 15. Growth rate and growth amount of airfoil and flap when $n=2$.

airfoil and the flap itself, respectively, this section divides the lift coefficient into two parts: the lift coefficient of the flap itself and the airfoil's lift coefficient that affected by the original split flap, that is $Cl_{OSF+airfoil} = Cl_{OSF} + Cl_{airfoil(OSF)}$; the airfoil with the curved flap are divided in the same way, and it is written as $Cl_{CFn+airfoil} = Cl_{CFn} + Cl_{airfoil(CFn)}$. When the curvature index is $n=2$, then it is written as $Cl_{CFn2+airfoil} = Cl_{CFn2} + Cl_{airfoil(CFn2)}$. By studying the lift coefficient of the flap itself and the lift coefficient of the airfoil affected by the flap, the influence mechanism of flap's curvature change on the lift coefficient is explored.

Figure 15(a) shows the growth rate of lift coefficient of the flap and the airfoil affected by flap when the curvature index $n=2$, and the calculation equations are (11) and (12), respectively:

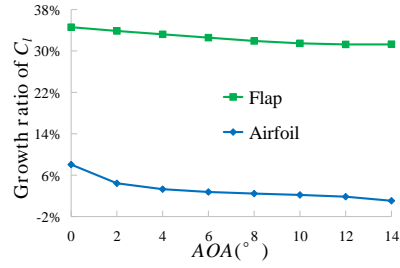
$$\frac{Cl_{CFn2} - Cl_{OSF}}{Cl_{OSF}} \quad (11)$$

$$\frac{Cl_{airfoil(CFn2)} - Cl_{airfoil(OSF)}}{Cl_{airfoil(OSF)}} \quad (12)$$

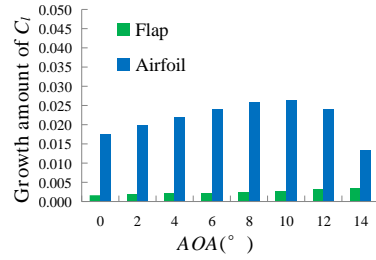
Figure 15(b) shows the growth amount of lift coefficient of the flap and the airfoil affected by flap when curvature index $n=2$, and the calculation equations are (13) and (14), respectively:

$$Cl_{CFn2} - Cl_{OSF} \quad (13)$$

$$Cl_{airfoil(CFn2)} - Cl_{airfoil(OSF)} \quad (14)$$

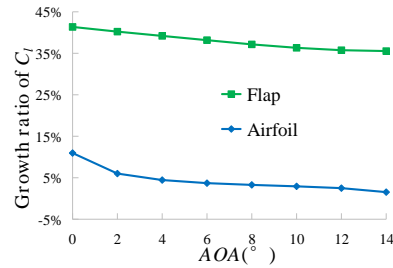


(a) Growth rate of lift coefficient

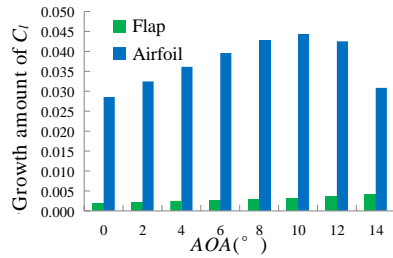


(b) Growth amount of lift coefficient

Fig. 16. Growth rate and growth amount of airfoil and flap when $n=4$.



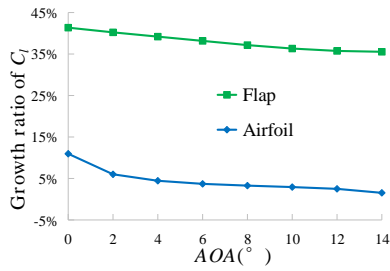
(a) Growth rate of lift coefficient



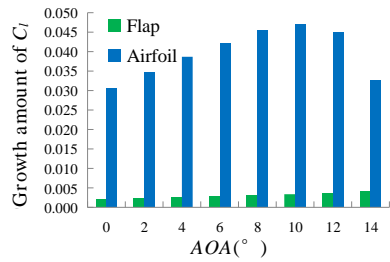
(b) Growth amount of lift coefficient

Fig. 17. Growth rate and growth amount of airfoil and flap when $n=8$.

Figure 16 to Fig. 18 establish the ordinate axis in the same way. It can be seen from Fig. 15(a), Fig. 16(a), Fig. 17(a) and Fig. 18(a) that when the curvature of the flap changes, the flap's lift coefficient changes dramatically. Besides, when $n=16$, the flap's lift coefficient can be increased by 43.56% at most. That is because the lift coefficient of the airfoil is indirectly affected by the change of the flap's curvature. The pressure nephogram in Fig. 19 also shows that, with the increase of flap's curvature index, the area of high pressure and pressure peak on the lower surface of the flap increase continuously. At the same time, there is only a relatively small



(a) Growth rate of lift coefficient



(b) Growth amount of lift coefficient

Fig. 18. Growth rate and growth amount of airfoil and flap when $n=16$

change of the pressure field around the airfoil. The above research results show that the change of flap's curvature has a greater impact on the flap itself than on the airfoil. However, because the ratio of flap's lift coefficient to airfoil's lift coefficient that affected by the flap is too small. Therefore, the growth of the overall lift coefficient is mainly caused by the change of lift coefficient of airfoil, the lift coefficient growth amount of flap is much smaller than that of airfoil at the same attack angle, as shown in Fig. 15(b), Fig. 16(b), Fig. 17(b) and Fig. 18(b).

According to section 4.1, a split flap can change the original flow direction of the airflow on the pressure surface and deflect the airflow downward, so as to change the pressure distribution of the airfoil integrated with flap by using the reaction force of the airflow. In this section, the principle that the curved split flap can further improve the lift based on the split flap in section 4.1 is analyzed. On the one hand, the airflow is blocked at the trailing edge of the flap, resulting in the growth of local surface pressure on the lower surface of the flap. Thus, the lift coefficient is improved, similar to the dolphin fluke propulsion principle on the bowl-shaped surface. On the other hand, as shown in Fig. 20(a) and 20(b), the airflow deflection angle at the trailing edge of curved flap β is greater than that of the original split flap α . However, it should be noted that the overall deflection angle of the two flaps is strictly guaranteed to be the same, both of which are α . When the airflow deflection angle is larger, the centripetal force required for airflow deflection is greater, which ultimately leads to the greater upward reaction force of airflow to the flap. Therefore, when the curvature index is higher, the peak value of the lower surface high-pressure area is greater, as shown in Fig. 19. The above two points are the main reasons the flap's lift coefficient increases after the flap changes its curvature.

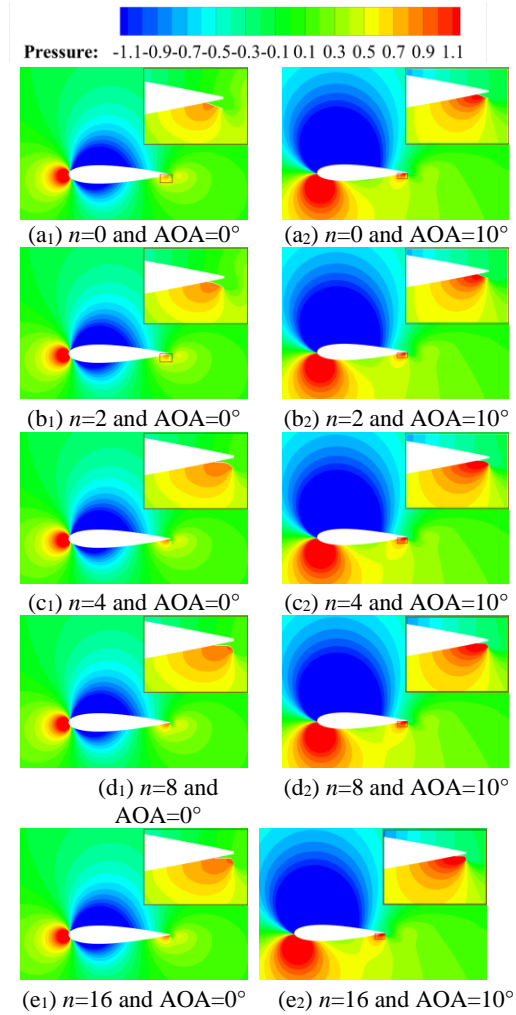


Fig. 19. Pressure distribution.

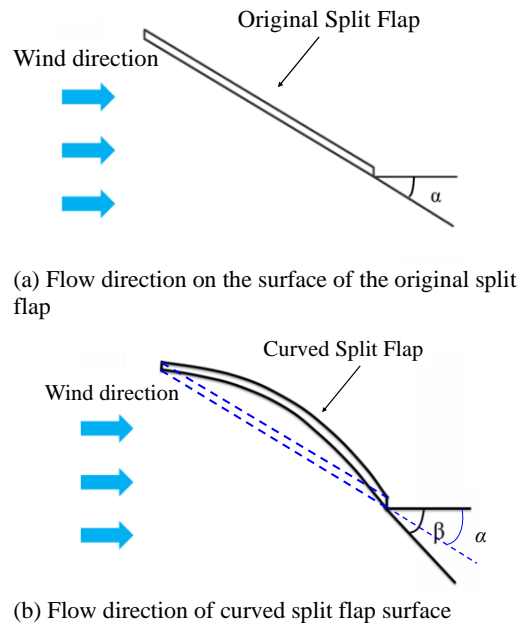


Fig. 20. Flow direction of original split flap and curved split flap.

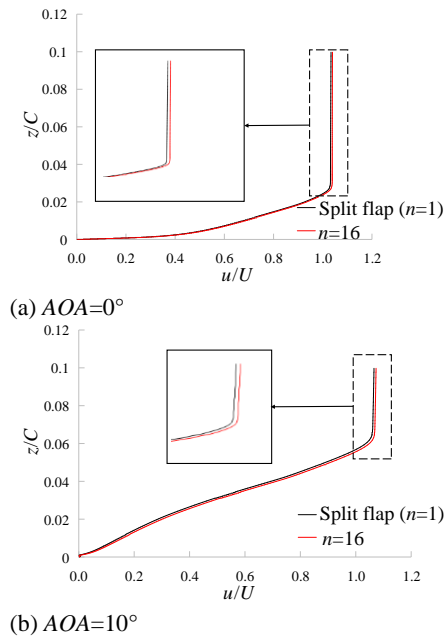


Fig. 21. Velocity distribution on suction surface of airfoil with curved flap ($x=0.9C$).

When the curvature of split flap is changed, the flap's lift coefficient is increased, and the airfoil's lift coefficient will also change under the influence of the flap. The change of the airfoil's lift coefficient is the fundamental reason for the rise of integral lift coefficient of airfoil with a flap as a whole.

Figure 21 shows the boundary layer velocity distribution of the airfoil's suction surface with original split flap and curved split flap ($n=16$) based on $90\%C$ of the airfoil, and the data results are normalized. As shown in Fig. 21, compared with the air velocity on the airfoil's suction surface with original split flap, the air velocity on the airfoil's suction surface with curved split flap is larger, which undoubtedly leads to the increase of the airfoil circulation and lift coefficient.

5. CONCLUSION

In this paper, based on the NACA0018 airfoil, by simulating the shape change of dolphin fluke during propulsion and based on the split flap, a curved split flap model with variable curvature is proposed. Meanwhile, the corresponding mathematical model is established. Through numerical simulation, the following conclusions are obtained:

- (1) In this paper, based on strictly ensuring the deflection angle of the original split flap and curved flap, it is found that when the flap is given a certain degree of curvature, the curved flap can further improve the aerodynamic characteristics of the airfoil and the original split flap.
- (2) The principle of curved flaps to optimize the aerodynamic characteristics of airfoils: on the one hand, the airflow is blocked on the lower surface of the flap, sharply increasing the local surface pressure, thus improving the overall lift coefficient,

which is very similar to the dolphin fluke propulsion principle on the bowl-shaped surface; on the other hand, although the precondition that the flap deflection angle remains unchanged is strictly guaranteed, the ability of the curved flap to deflect the airflow at the trailing edge is enhanced by rearranging the local deflection angle of the traditional flap.

(3) When the curvature index n of split flap is greater, the lift-rising effect is more pronounced and gradually tends to a constant value. In this paper, when the curvature index is $n=16$, the lift coefficient (C_l) and the lift-to-drag ratio (C_l/C_d) can be increased by 15.05% and 12.75%, respectively, based on the original split flap.

(4) By changing the curvature index of the flap, it is found that the flap's lift coefficient growth rate is much larger than that of the airfoil affected by the original split flap. However, the fundamental reason for the change of the whole lift coefficient is that the flap effects the growth of the airfoil's lift coefficient.

(5) In the follow-up research, the length L and the height H of flap could be further optimized under the premise that the resistance change is not obvious, so as to further improve the lift coefficient and lift-to-drag ratio of the airfoil integrated with the flap.

ACKNOWLEDGEMENTS

This work was funded by Shanghai Rising-Star Program (Grant No. 19QC1400200), and the foundation of National Key Laboratory of Science and Technology on Aerodynamic Design and Research (Grant No. 6142201200314).

REFERENCES

- Atalay, K. D., B. Dengiz, T. Yavuz, E. Koç and Y. T. İç (2020). Airfoil-slat arrangement model design for wind turbines in fuzzy environment. *Neural Computing and Applications* 32, 13931-13939.
- Bénard, N., J. Jolibois and E. Moreau (2009). Lift and drag performances of an axisymmetric airfoil controlled by plasma actuator. *Journal of Electrostatics* 67(2), 133-139.
- Bianchini, A., F. Balduzzi, D. Di Rosa and G. Ferrara (2019). On the use of Gurney Flaps for the aerodynamic performance augmentation of Darrieus wind turbines. *Energy Conversion and Management* 184, 402-415.
- Daróczy, L., M. H. Mohamed, G. Janiga and D. Thévenin (2014). Analysis of the effect of a slotted flap mechanism on the performance of an H-Darrieus turbine using CFD. In *Turbo Expo: Power for Land, Sea, and Air*, American Society of Mechanical Engineers.
- Duong, N. T., M. Kashitani, M. Taguchi, K. Kusunose and Y. Takita (2020). Study on Aerodynamic Characteristics of Supersonic Biplane installed Split Flap by Wake

- Measurement. In *AIAA Scitech 2020 Forum*, Orlando, America, 0536.
- Fatahian, E., A. L. Nichkoochi, H. Salarian and J. Khaleghinia (2019). Comparative study of flow separation control using suction and blowing over an airfoil with/without flap. *Sādhanā* 44(11), 220.
- Feero, M. A., P. Lavoie and P. E. Sullivan (2017). Influence of synthetic jet location on active control of an airfoil at low Reynolds number. *Experiments in Fluids* 58(8), 99.
- Fish, F. E., T. M. Williams, E. Sherman, Y. E. Moon, V. Wu and T. Wei (2018). Experimental measurement of dolphin thrust generated during a tail stand using DPIV. *Fluids* 3(2), 33.
- Huang, S., Y. Hu and Y. Wang (2021). Research on aerodynamic performance of a novel dolphin head-shaped bionic airfoil. *Energy* 214, 118179.
- Kaul, U. K. and N. T. Nguyen (2014). Drag optimization study of variable camber flap continuous trailing edge flap (VCCTEF) using OVERFLOW. In *32nd AIAA Applied Aerodynamics Conference*, Atlanta, America.
- Kim, N., M. Han, A. Iakovleva, H. Park, W. Chu and S. Ahn (2020). Hybrid Composite Actuator with Shape Retention Capability for Morphing Flap of Unmanned Aerial Vehicle (UAV). *Composite Structures* 112227.
- Kral, L. D. (2000). Active flow control technology. *ASME Fluids Engineering Technical Brief* 1-28.
- Kulhánek, R., Z. Pátek, P. Vrchota, P. Procházka and V. Uruba (2020). Experimental and CFD study of slotted Krueger flaps aerodynamics in critical locations. *International Journal of Numerical Methods for Heat and Fluid Flow* 31(2), 618-628.
- Kumar, Y., M. Paraschivoiu and I. Paraschivoiu (2010). Low reynolds number vertical axis wind turbine for mars. *Wind Engineering* 34(4), 461-476.
- Li, C. X., C. Zhang, R. X. Zhang and X. M. Ye (2020). Effect of gurney flap on performance and aeroacoustics of variable-pitch axial fans. *AIAA Journal* 58(6), 2546-2559.
- Liebeck, R. H. (1978). Design of subsonic airfoils for high lift. *Journal of Aircraft* 15(9), 547-561.
- Liu, Y. and L. Tan (2018). Method of C groove on vortex suppression and energy performance improvement for a NACA0009 hydrofoil with tip clearance in tidal energy. *Energy* 155, 448-461.
- Melton, L. P., N. W. Schaeffler, C. Yao and A. Seifert (2005). Active control of flow separation from supercritical airfoil leading-edge flap shoulder. *Journal of Aircraft* 42(5), 1142-1149.
- Pawsey, N. C. K. (2002). *Development and Evaluation of Passive Variable-Pitch Vertical Axis Wind Turbines*. Ph. D. Thesis, University of New South Wales, Sydney, Australia.
- Post, M. L. and T. C. Corke (2006). Separation control using plasma actuators: dynamic stall vortex control on oscillating airfoil. *AIAA journal* 44(12), 3125-3135.
- Schaefer, L. (2008). Fin structure and function. <https://understanddolphins.tripod.com/dolphinfinstructurefunction.html>.
- Urnes, J. and N. Nguyen (2013). A mission adaptive variable camber flap control system to optimize high lift and cruise lift to drag ratios of future n+3 transport aircraft. In *51st AIAA Aerospace Sciences Meeting including the New Horizons Forum and Aerospace Exposition*, Dallas, America, 0214.
- Velasco, D., O. L. Mejia and S. Laín (2017). Numerical simulations of active flow control with synthetic jets in a Darrieus turbine. *Renewable Energy* 113, 129-140.
- Wang, H., B. Zhang, Q. Qiu and X. Xu (2017). Flow control on the NREL S809 wind turbine airfoil using vortex generators. *Energy* 118, 1210-1221.
- Wang, Y., G. Li, S. Shen, D. Huang and Z. Zheng (2018). Influence of an off-surface small structure on the flow control effect on horizontal axis wind turbine at different relative inflow angles. *Energy* 160, 101-121.
- Weick, F. E. and R. C. Platt (1933). Wind-tunnel tests on model wing with fowler flap and specially developed leading-edge slot. *NASA Technical Reports Server* 1-30.
- Zhang, L., J. Gu, K. Hu, H. Zhu, J. Miao, X. Li and Z. Wang (2021). Influences of trailing edge split flap on the aerodynamic performance of vertical axis wind turbine. *Energy Science and Engineering* 9(1), 101-115.
- Zhang, W., Z. Zhang, Z. Chen and Q. Tang (2017). Main characteristics of suction control of flow separation of an airfoil at low Reynolds numbers. *European Journal of Mechanics-B/Fluids* 65, 88-97.
- Zhou, Y., L. Hou and D. Huang (2017). The effects of Mach number on the flow separation control of airfoil with a small plate near the leading edge. *Computers and Fluids* 156, 274-282.
- Zhu, H., W. Hao, C. Li and Q. Ding (2019). Numerical study of effect of solidity on vertical axis wind turbine with Gurney flap. *Journal of Wind Engineering and Industrial Aerodynamics* 186, 17-31.